SIWI STOCKHOLM JUNIOR WATER PRIZE

Entry to the Stockholm Junior Water Prize 2025

AI-Optimized Hydrogel-Zeolite Photocatalytic Wastewater Purifier

Egypt

Adam Ahmed El-Hussiny Salama, Ahmed Hosny Eldeeb

Key words: Hydrogel, Zeolite, Photocatalysis, Desalination, Water Treatment, Solar Energy

TABLE OF CONTENT

APS – Ammonium persulfate
CB – Conduction band
COD – Chemical oxygen demand
ESP32 – Low-power Wi-Fi/Bluetooth microcontroller
g-C_3N_4 – Graphitic carbon nitride
MBA – N,N'-methylenebisacrylamide
MB – Methylene blue
PONI – Polyaniline
PVA – Poly(vinyl alcohol)
PSA – Poly(sodium acrylate)
ROS – Reactive oxygen species
SA – Sodium acrylate
TDS – Total dissolved solids
TiO_2 – Titanium dioxide
UV – Ultraviolet
UV-254 – Ultraviolet absorbance at 254 nm
VB – Valence band
WHO – World Health Organization
ZA – Zeolite A

PROJECT SUMMARY

Severe water scarcity in off-grid desert-edge and coastal communities requires desalination methods and contamination removal that are independent of energy-intensive such as reverse osmoses methods that requires about 3 to 5.5 kWh per cubic meter of water. This solution presents a cost-effective, solar-powered system designed to remove a wide range of contaminants then desalinate it by distillation. synthetic zeolite A, synthesized from kaolinite, adsorbs heavy metals and minimizes the chemical oxygen demand (COD). Concurrently, an osmotic-pressure-driven hydrogel formed from poly sodium acrylate, methylenebisacrylamide, ammonium persulfate for absorbing water and making salt rejection, and polyaniline for enhancing light absorption incorporated in a loofah sponge. The 3D pores structure of the loofah efficiently transports water to the evaporation area by osmotic pressure. Also, it prevents salt accumulation through negative charge groups of the hydrogel materials. While titanium dioxide (TiO2) photocatalysis under the sun targets organic contaminants such as dyes; these materials will increase the lifespan of the hydrogel as it protects the hydrogel from degradation. Under 1-sun irradiation, Zeolite A removed up to 90% of COD in 30 minutes, which surpasses the 80% removal by natural zeolite in 50 minutes, and the PSA/PONI/Loofah hydrogel achieved evaporation rates reaching 2.8 kg m^{-2} h^{-1}. Titanium dioxide (TiO2) was used as a photocatalyst to evaluate a baseline degradation efficiency of methylene blue under normal sunlight as well as a shaded region; it achieved approximately 77.5% adjusted efficiency, with 10.4% in the shade. Overall, this hybrid hydrogel–zeolite–photocatalyst system is a practical and scalable method of solar-powered water purification. It has the potential to address water scarcity and contamination in varied environments, potentially improving access to clean water globally.

INTRODUCTION

Every hour, the Sahara captures 2.5 TWh of solar energy, which is more than Africa's largest desalination plant uses in a day **(Vatansever, 2024)**. Although rural communities along its fringes rely on brackish wells or seawater. Because of the high cost required for the infrastructure of reverse osmosis systems to convert sunlight into electricity (> 3 kWh m^{-3}).

In recent years, solar-driven interfacial desalination has emerged as a sustainable alternative by localizing solar heating at thin layer called air-water interface, improving evaporation efficiency while minimizing heat loss to bulk water **(Hu *et al.*, 2024)**. Building on this principle, hydrogel-based solar evaporators have gained attention for next-generation desalination systems as an inexpensive solar desalination process. Hydrogels are water-absorbing polymers that reduce the energy required for evaporation **(Zhou *et al.*, 2020)**, particularly when combined with photothermal materials (e.g., carbon-based or plasmonic nanoparticles) that convert sunlight into heat. Research has demonstrated high evaporation rates using hydrogel designs that optimize water transport via capillary action and osmotic pressure **(Chen *et al.*, 2023).**

Beyond desalination, zeolites—crystalline aluminosilicate minerals with uniform pores—are also significant in water treatment for ion exchange and molecular sieving. Natural zeolites may have limited adsorption capacities or impurities, but synthetic variants offer more consistent pore sizes and higher purity. Additionally, photocatalysts like titanium dioxide (TiO_2) or doped TiO_2 are used to degrade organic pollutants and mitigate bacterial growth in water filters **(Arun et al., 2023; Budiarso et al., 2024)**

A. **Research Question** How can a combined system of hydrogel-based solar desalination and zeolite- and photocatalyst-enhanced water treatment be developed to efficiently address freshwater scarcity while minimizing energy use and maximizing pollutant removal at low cost?
B. **Purpose/Goal**

1) Optimize Hydrogel-Based Solar Desalination: Investigate how integrating osmotic pressure-driven water transport and photothermal materials can improve evaporation rates.

2) Enhance Water Purification: Examine the role of zeolites for ion exchange and photocatalysts (e.g., doped TiO2) for breaking down organic pollutants, aiming for a comprehensive water treatment approach.

3) Develop a Cost-Effective, Scalable System: Combine these technologies into a single, efficient framework suitable for resource-limited areas with high solar potential. If this project is a continuation of earlier work on hydrogel design or water purification, this year's focus is on merging these separate elements—hydrogel desalination and advanced filtration using zeolites and photocatalysts—into a cohesive system that can be tested under realistic conditions.

BACKGROUND AND LITERATURE REVIEW

Different hydrogel evaporators have been developed by researchers to enhance the performance of solar desalination. For example, a polyvinyl alcohol (PVA) polypyrrole (PPy) hydrogel achieved approximately ~3.2kgm^{-2} h^{-1} under one-sun irradiation. This high performance is attributed to the three dimensionally hierarchical pore structure of hydrogel, which promotes water transport to the evaporation surface via capillary action. The micro- and nano-channels ensure continuous water supply, preventing a drying zone even under strong heating, but materials like PPY are expensive to use in large scale. A similar phenomenon was observed in a three-dimensional chitosan hydrogel/loofah. The loofah hydrogel's hydrophilic nature and water-absorbing properties increased the evaporation rate, but it achieved law evaporation rate about 2kgm^{-2} h^{-1} **(Gao et al., 2024; Wang et al., 2023; Yue et al., 2023).**

1) Water Transport Mechanisms in Hydrogel

Hydrogels transport water through two mechanisms:

• **Capillary Action:** Water is drawn into the porous hydro gel due to cohesive and adhesive forces. However, salt clogging may eventually reduce performance.

• **Osmotic Pressure:** A high osmotic-strength polyelectrolyte hydrogel generates significant osmotic pressure, pulling water from the low-osmotic (bulk water) region to the high-osmotic (hydrogel) region. Negatively charged groups within the hydrogel repel negatively charged ions, preventing salt infiltration. Together, these mechanisms enable continuous hydration and maintain high evaporation rates **(Wang et al., 2023)**.

2) Photothermal Materials

To enhance the evaporation rate, photothermal materials such as carbon-based agents (black carbon nitride, graphene oxide) and plasmonic agents (gold, silver) improve light to-heat conversion. This increased thermal efficiency under sunlight further boosts evaporation performance.

Zeolite-Based Ion Exchange

Zeolites are crystalline aluminosilicates whose AlO_4 and SiO_4 tetrahedra form uniform molecular-sieve pores. Their negatively charged framework enables cation exchange, trap ping contaminants (e.g. Pb^{+2}, NH^{+}) by swapping them for Na^{+} (Dehmani 2024). 4 1) Natural vs. Synthetic Zeolites: Natural zeolites often exhibit:

• Lower adsorption capacity and variable composition (impurities)

• Restricted pore sizes limiting uptake of larger molecules Synthetic zeolites offer:

1- Tailored pore structures and higher purity
2- Enhanced thermal/chemical stability
3- Greater, consistent ion-exchange capacity

Photocatalytic Enhancement

Photocatalysts accelerate light-driven reactions without be- ing consumed (Puri Gupta 2023). Titanium dioxide (TiO_2) breaks down organics under UV; doping with metals (Fe, Cu)

or non-metals (N, S) shifts its bandgap into the visible range, boosting solar efficiency and enabling self-regenerating water filters **(**Arun 2023**), (**Budiarso 2024**)**.

Titanium Dioxide Photocatalysis Mechanism

Titanium dioxide (TiO2) is a semiconductor with a bandgap of 3–3.2 eV. When UV light of energy hv ≥ Eg falls on TiO2, electrons are excited from the valence band (VB) to the conduction band (CB), generating electron–hole pairs:

$$TiO_2 + h\nu \longrightarrow e^-_{CB} + h^+_{VB}.$$

These charge carriers interact with adsorbed oxygen and water to form reactive oxygen species (ROS), which then degrade pollutants or microbes.

The primary ROS are:

• **Hydroxyl radicals:** ·OH

• **Superoxide anions:** O2

– The key reactions for ROS generation are:

$$e^-_{CB} + O_2 \longrightarrow O_2^{\cdot -},$$
$$h^+_{VB} + H_2O \longrightarrow \cdot OH + H^+.$$

Overall, This project hopes to provide a solution to global freshwater scarcity by consolidating the advantages of these proven processes into a singular, scalable treatment system that is cost-effective and energy-efficient.

METHODOLOGY

Loofah sponge were treated by dispersing it in water for 12 hours to remove any natural oils, then sonicating it in DI water for 30 minutes to further clean the porous structure, and then immersing it in 0.5M NaOH solution at 60°C for 2 hours to increase it is hydrophilicity, and rinsing them thoroughly with DI water until the pH was neutral (Figure a). After that,

sodium acrylate was prepared by mixing acrylic acid 99% with 6 M NaOH in a 1:1 ratio (Figure b). Sodium acrylate (SA, 99%), N,N'-methylenebisacrylamide (MBA, 99%) (cross-linker), and ammonium persulfate (APS, 98%) (thermal initiator) were dissolved in water by a molar ratio of 50:1:1 to obtain a 20% homogeneous solution. The treated loofah immersed in the solution overnight to ensure that the pores in the loofah were filled with solution. PONI was dissolved in 5% PVA solution by a ratio of 1:0.2 by weight (Figure c). The PSA-based loofah was immersed in PONI solution from one side for 1 h. After which it was put into an oven at 70 °C for 2 h for copolymerization of SA (Figure d).

Figure 1. *Steps of making PSA/PONI/Loofah based hydrogel*

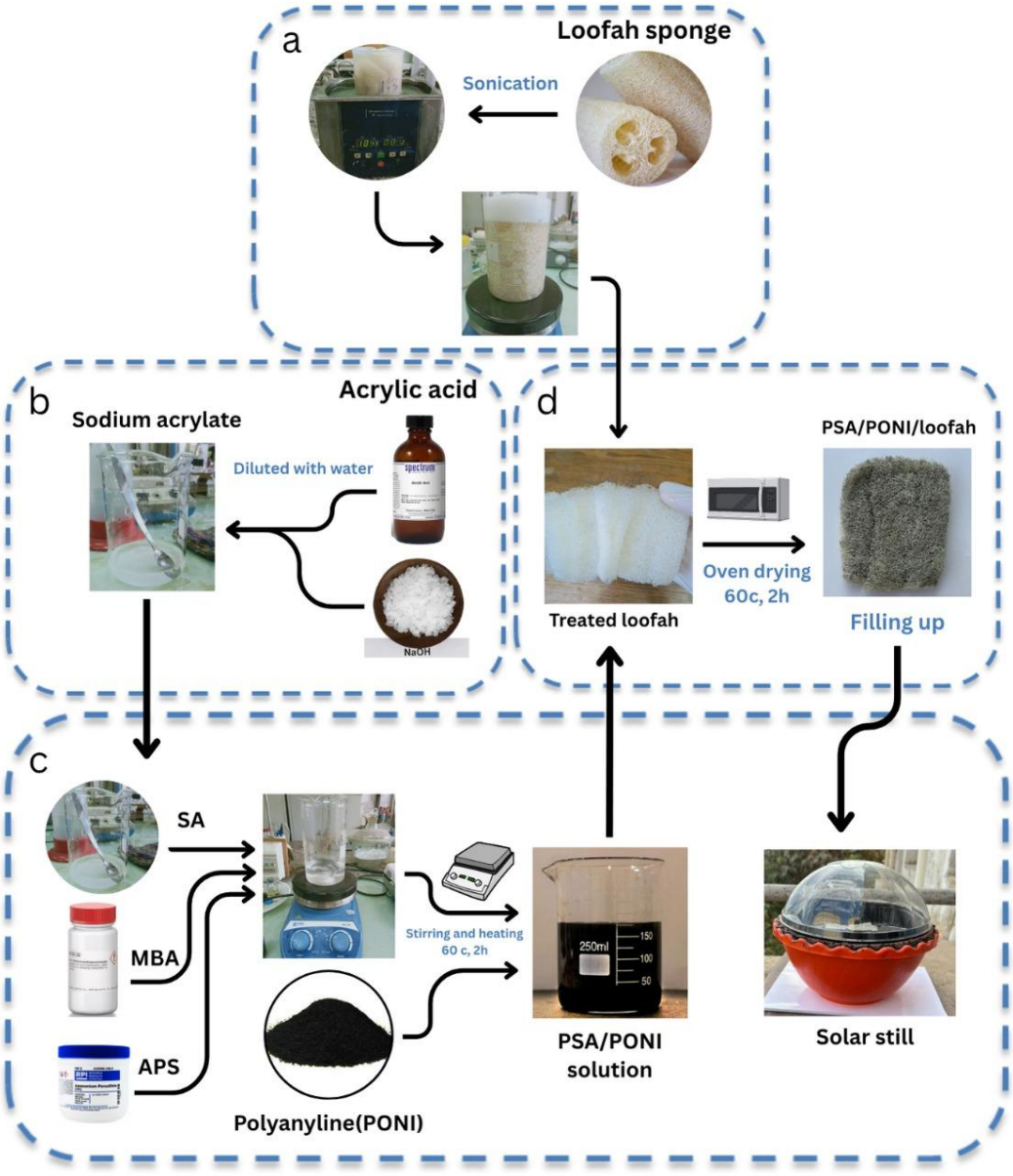

Hydrogel Performance Testing

1) **Evaporation Rate Measurement:** PSA/PONI/Loofah based hydrogel was placed in a petri dish containing 3.5 wt% NaCl solution to simulate seawater. A precision balance (±0.001 g accuracy) recorded mass loss every 15 minutes under 1-sun irradiation (1 kW/m2) from the natural sunlight. Evaporation rates ($g \cdot m^{-2} \cdot h^{-1}$) were calculated using:

$$\text{Evaporation Rate} = \frac{\text{Mass Loss (g)}}{\text{Area (m}^2\text{)} \times \text{Time (h)}}.$$

2) **Water Absorption and Transport Analysis:** The hydro- gels were immersed in DI water to determine swelling ratios (percent weight increase over time). This analysis was used to compare water uptake between PVA–PONI and PSA/PONI/Loofah hydrogels samples.

3) **Salt rejection:** Salt rejection efficiency was determined as follows. The dry mass of the hydrogel ($m_{dry,0}$) was measured as 4.5 g then it immersed in a 3.6 wt% NaCl solution for 24 h To resemble seawater. ($m_{wet,0}$) =23 g, and the absorbed water mass is $\mathbf{\Delta m_{abs} = m_{wet} - m_{dry,0} = 18.5\ g}$. After re-drying to a constant mass $m_{dry,1}$=4.662 g, the salt uptake is $\mathbf{\Delta m_{salt} = m_{dry,1} - m_{dry,0}}$=0.162 g. Assuming a maximum possible salt ingress of 0.035 Δm_{abs}, the salt rejection efficiency is:

$$\eta_{SR} = 1 - \frac{\Delta m_{salt}}{0.035\, \Delta m_{abs}}.$$

η_{SR} = 1 – 0.162 g / 0.648 g = 0.75 (75 %). So, the salt held in the hydrogel is about **8 800 ppm,** four times less salty than the surrounding water which ranges from **35–36 000 ppm**.

C. Zeolite Adsorption Experiments

1) Comparison of Natural and Synthetic Zeolites: Natural zeolite (NZ) and synthetic zeolite A (ZA) were tested for pollutant adsorption from wastewater. Wastewater samples were analyzed for initial chemical oxygen demand (COD) using a spectrophotometer. Different masses of zeolite (0.05–0.3 g) were added to separate wastewater samples to investigate the effect of dosage.

2) Contact Time and COD Measurement: Adsorption was performed under varying contact times (10, 20, 30, 40, 50 minutes) to determine the optimum duration for COD reduction. After each specified contact time, COD was measured again to evaluate pollutant removal efficiency. This process helped identify the best-performing zeolite type and dosage.

D. Photocatalytic Degradation with Titanium Dioxide

1) Methylene Blue Preparation: A 10 ppm methylene blue (MB) solution was prepared by dissolving approximately 2.4 mg of MB in 200 mL of DI water. The solution was then split equally into two 100 mL beakers.

2) TiO2 Addition and Setup: To each 100 mL portion, 0.1 g of TiO2 was added and stirred thoroughly. One beaker was placed in direct sunlight, while the other was kept in the shade, maintaining similar conditions except for light exposure.

3) Data Collection: Samples (2–3 mL) were withdrawn every 30 minutes over a 3-hour period (11 A.M.–2 P.M.). After filtering out TiO2, absorbance was measured at 664 nm using a UV–Vis spectrophotometer. The initial absorbance served as the baseline to determine the percentage of MB degradation over time.

E. Synthesis of Graphitic Carbon Nitride (g-C3N4)

1) g-C3N4 Preparation: A homogeneous solution was made by dissolving 15 g of urea in 20 mL of DI water and stirring for 30 minutes. This mixture was heated to 673 K for 2 hours to allow urea to decompose and polymerize into a solid product. The temperature was then raised to 723 K for another 2 hours in a semi-enclosed porcelain crucible, burning off excess carbon and forming g-C3N4

2) Testing with Zeolite A and g-C3N4: Subsequent experiments compared the adsorption or photocatalytic performance of zeolite A and the synthesized g-C3N4 under various conditions, such as pollutant type and contact time, using COD measurements and spectrophotometric analysis.

F. Equipment Used

- **Precision Balance (±0.001 g):** To record mass loss during evaporation experiments
- **Spectrophotometer/UV–Vis:** For measuring COD (in wastewater) and absorbance of methylene blue solutions
- **Magnetic Stirrer:** Used during polymerization and mixing steps
- **Vortex Mixer:** To ensure uniform dispersion of reagents
- **Porcelain Crucible and Furnace:** For synthesizing g- C3N4
- **Beakers and Petri Dishes:** For sample containment and testing setups

RESULTS AND DISCUSSION

In this section, we present and discuss the findings from the hydrogel swelling tests, slat rejection, evaporation rate measurements, COD removal experiments, and photocatalytic degradation trials.

A. Hydrogel's water absorption

The swelling ratio of the PSA/PONI/loofah-based hydrogel was measured over time to observe its water absorption capacity. Table I shows the recorded mass at different time intervals after immersion in deionized water. The hydrogel exhibits high initial water uptake in the first 30 seconds (Table 1,2), with a 4.22 swelling ratio, followed by a gradual increase in swelling ratio in comparison to other hydrogels like PVA-PONI, which achieved a 3.22 swelling ratio after 45 minutes. This behavior underscores the hydrogel-based loofah's strong hydrophilic nature, making it suitable for desalination applications that require continuous water absorption.

Table I.

Water absorption of PSA/PONI/Loofah hydrogel

Time (min)	Mass (g)	Swelling Ratio
0	4.5	0
0.5	19.00	4.22
1	20	4.44
2	20.5	4.56
5	21	4.67
10	21.8	4.84
20	22.5	5.00
40	23	5.11

Table II.

Water absorption of PVA/PONI hydrogel

Time (min)	Mass (g)	Swelling Ratio
0	0.97	0
5	2.45	2.51
7.5	2.68	2.77
10	2.78	2.87
12.5	2.85	2.95
20	2.92	3.02
35	2.06	3.17
45	3.114	3.22

Figure 2. *Dry PSA/PONI/Loofah*

Figure 3. *Wet PSA/PONI /Loofah after 30 seconds*

Figure 4. *Dry PVA/PONI hydrogel*

Figure 5. *Wet PVA/PONI hydrogel after 45 minutes*

B. Hydrogel's Salt Rejection

The hydrogel achieved 75% salt rejection. This high rejection arises from the osmotic pumping effect of PSA, which draws water from the lower-osmotic bulk into the higher-osmotic hydrogel and repels salt ions via its charged groups.

Hydrogel's Water Evaporation

The hydrogel achieved E ≈ 2.8 kg m−2 h−1, thanks to PONI's high photothermal conversion and continuous water transport to the evaporation surface. Furthermore, effective salt rejection prevents fouling, maintaining consistent evaporation efficiency over time.

Figure 7. *Water evaporation of the hydrogel overtime*

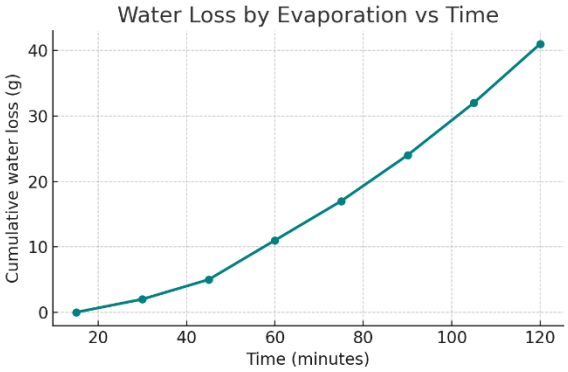

Figure 8. *Solar still in the first of evaporation process*

Figure 9. *Solar still after two hours of evaporation process*

D. COD Removal and Photocatalytic Degradation

1) Zeolite Adsorption Performance: Natural zeolite (NZ) and synthetic zeolite A (ZA) were used to remove contaminants from wastewater samples, measured by chemical oxygen demand (COD). Figures 11 and 10 illustrate the COD removal efficiency as a function of zeolite dosage and contact time, respectively. Synthetic Zeolite A: in just 30 minutes it drove the COD down from 537 mg L^{-1} to 52 mg L^{-1}, an ≈ 90 % reduction.Natural Zeolite: over 50 minutes it lowered the COD from 512 mg L^{-1} to 103 mg L^{-1}, about an 80 % drop.

2) Photocatalytic Degradation of Methylene Blue: Titanium dioxide (TiO2) was used as a photocatalyst to degrade methylene blue (MB) under sunlight and shaded conditions. Figures 14 and 13 show the absorbance data at 664 nm over time. The initial absorbance served as a baseline to calculate the percentage of dye degradation.

Figure 10. *COD Removal by Contact Time.*

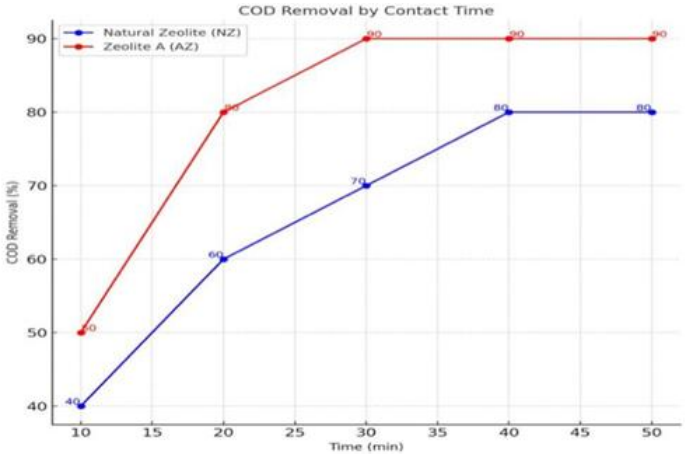

Figure 11. *COD Removal by Zeolite Dose.*

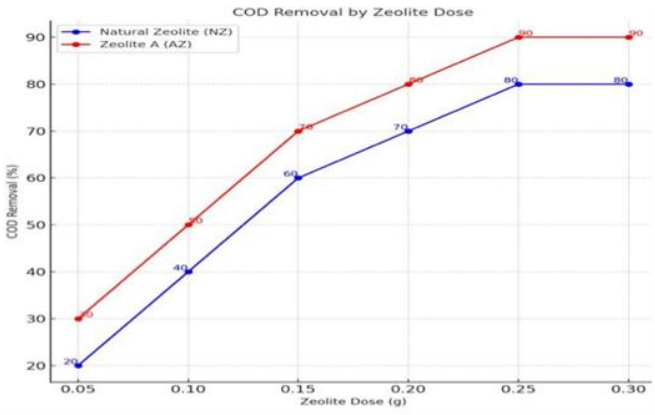

Figure 13. *Absorbance vs. Time under Sunlight.*

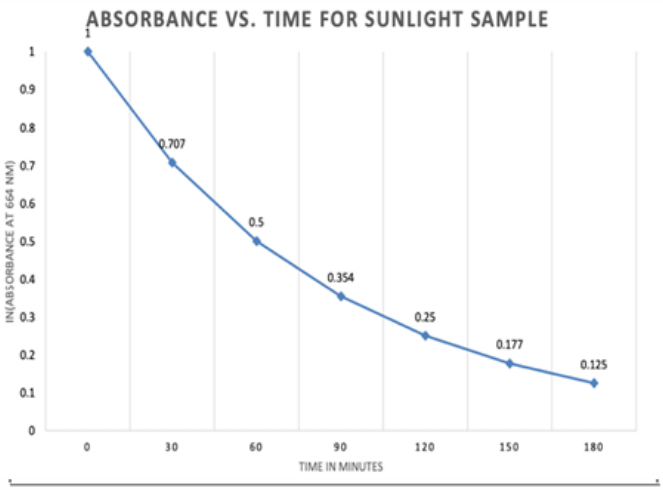

Figure 14. *Absorbance vs. Time in Shade.*

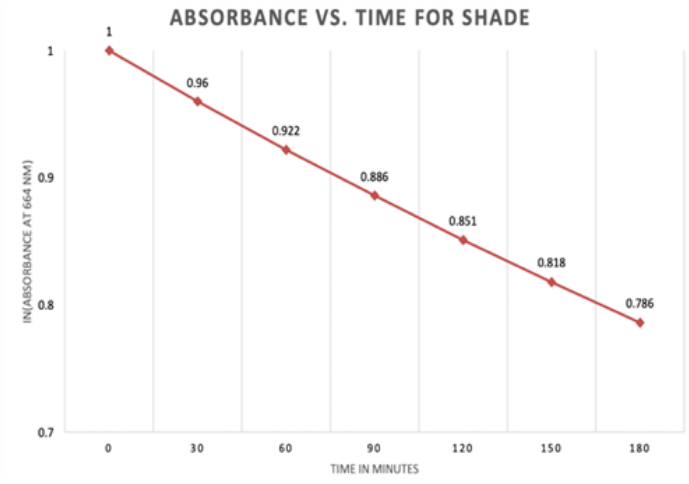

E. Additional Observations and Illustrations

XRD Analysis and Morphological Observations: We performed X-ray Diffraction (XRD) on our sample to identify its mineralogical composition. Cu Kα radiation (λ = 1.5406 A˚) was used, scanning from 2θ = 2.00◦ to 60.00◦ with a 0.020◦ step size (0.4 s per step) at 25◦C.

Peak Identification and d-Spacing Calculations: Distinct diffraction peaks appear at 2θ ≈ 7.18◦, 10.10◦, 12.42◦, 24.00◦, and others Using Bragg's law (Eq. 1, with n = 1),

$n\lambda = 2d \sin \theta,$

we obtained the interplanar spacings, e.g. d ≈ 12.3 A ˚ (2θ = 7.18◦), d ≈ 8.8 A ˚ (2θ = 10.10◦), d ≈ 7.1 A ˚ (2θ = 12.42◦), and d ≈ 3.7 A ˚ (2θ = 24.00◦). These values match Zeolite A's LTA framework. Comparison with Standard Data: Calculated d–spacings and peak positions were compared with the International Zeolite Association (IZA) database, confirming the sample as Zeolite A.

Crystallite Size Estimation: To estimate crystallite size we applied the Debye–Scherrer equation (Eq. 2):

$D = K\lambda \beta \cos \theta$, (2) where K = 0.9 and β = 0.1◦ (in radians). Using the primary peaks (2θ = 7.18◦, 10.10◦, 12.42◦, 24.00◦), we obtained D ≈ 79 nm. These nanoscale crystallites aggregate into the 900–1320 nm cubic particles observed in SEM images (14 crystallites per particle). Graphitic Carbon Nitride Sample: For the g-C3N4 sample, Bragg's Law gave d ≈ 6.64 A ˚ at 2θ = 13.1◦ and d ≈ 3.24 A ˚ at 2θ = 27.4◦. Debye–Scherrer analysis yielded crystallite sizes of ∼ 159.5 nm (13.1° peak) and ∼ 100.3 nm (27.4° peak), consistent with the layered structure of g-C3N4

Figure 15. *SEM micrograph illustrating zeolite A's crystalline and porous nature*.

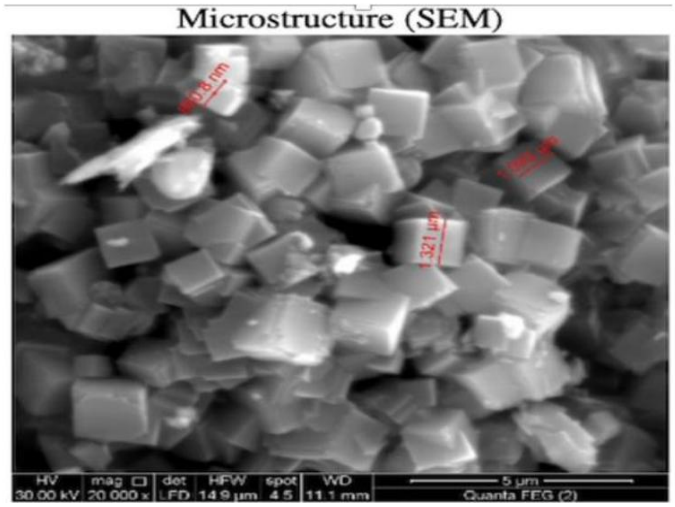

Figure 16. *Powder X-Ray Diffraction (PXRD) pattern of zeolite A sample*

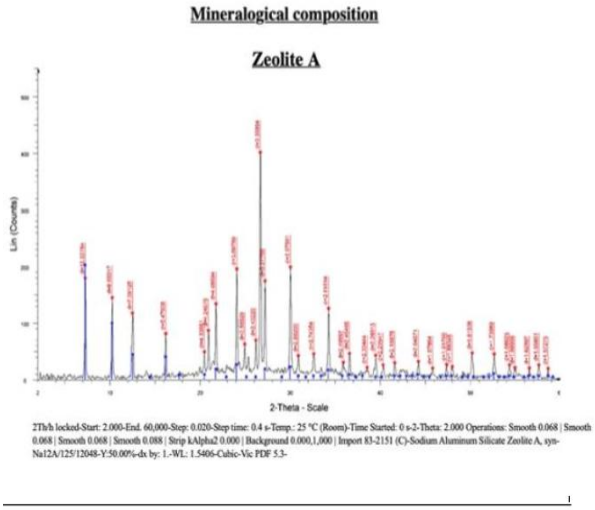

Figure 17.*XRD Micrograph of the graphitic carbon nitride sample (g-C3N4)*

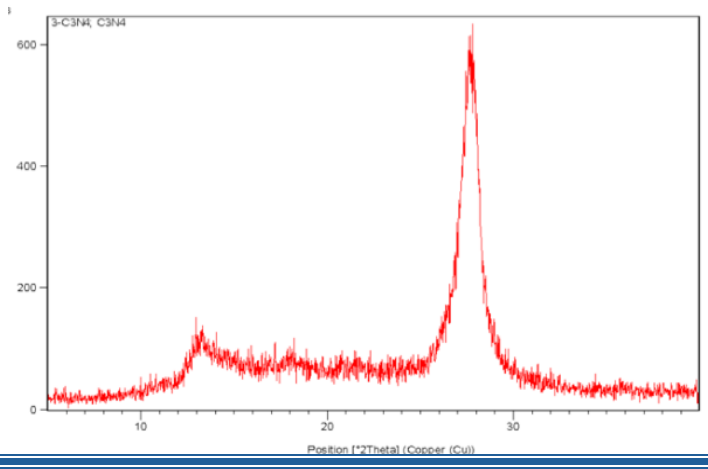

Figure 18. *Compositional Profiling and Peak Deconvolution of LTA-Framework*

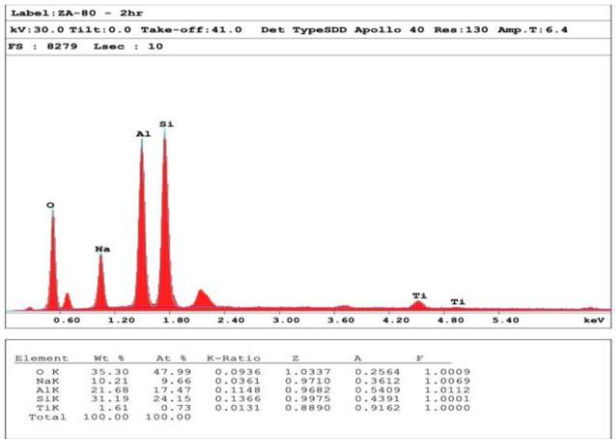

A.Three-Step Water Treatment Process The water purification

The system operates in three consecutive stages:

Figure 19. *Three stage water treatment system*

1) Coagulation: alum and moringa solution dosed into the raw water. The alum-moringa complexes with suspended solids and microorganisms, forming heavy flocs that settle to the bottom of the tank.

2) Filtration: The clarified water is passed through a mixed bed of sand filter and Zeolite A, first sand filter removes the remaining suspended particles at\ the water and Zeolite A removes toxic metal ions via ion exchange to leave the water with salt now free from any contamination that may degrade the hydrogel.

3) Solar Hydrogel Distillation: The filtered water is wicked into a loofah sponge impregnated with a specialized hydrogel. rejecting most dissolved salts. The vapor is then condensed to produce salt-free water. TiO2/g-C3N4 particles, activated by sunlight, generate reactive species that degrade organic residues increasing hydrogel's life span.

B. System Monitoring and Control We monitor the treatment unit with a set of simple sensors:

• Turbidity and flow meters upstream and downstream of the settling stage.

• TDS sensor on the water line exiting the filter. All sensor outputs are routed to an ESP32 control board, which logs real-time measurements.

• Adjusts pump speed and alum-moringa dosing when readings deviate from setpoints.

• Performs rapid self-checks to maintain sensor accuracy. This straightforward feedback loop ensures continuous production of clear, low-salinity water—even in remote, off-grid installations.

. *Research Plan for a Self-Learning Purifier*

1) Enhanced Data Collection: Continue logging all ex- isting sensor measurements (turbidity, TDS, pH, color, iron, manganese, water temperature) and add:

- Ambient sunlight level
- Flow rate

2) Neural-Network Controller: Train a lightweight neural network with two subnetworks:

- *Treatment selector:* Chooses between zeolite, hydro- gel, or both.
- *Dosage estimator:* Predicts the optimal chemical dose.

The model will perform nightly updates using that day's logged data, avoiding the need for retraining from scratch.

3) Confidence Monitoring: If the network's output falls below a confidence threshold, flag the decision for human review.

4) Closed-Loop Feedback: After dosing, compare new sensor readings to WHO water quality limits. Compute the dosing error and feed it back into the network to refine future predictions.

5) Performance Metrics: Track over a six-month pilot:

- Mean dosage error
- Treatment success rate
- Total chemical consumption

Target at least **15% reduction** in chemical usage com- pared to current trial-and-error protocols.

By continuously learning from each batch while preserving operator oversight, this approach aims for a fully automated, adaptive purification system without sacrificing transparency.

Conclusion

This study demonstrates that a bioderived hydrogel unites loofah microchannels, a poly(sodium-acrylate) osmotic network, and a polyaniline photothermal skin can convert ordinary sunlight into clean water with both high flux and effective salt resistance. The material reaches a steady evaporation rate of 2.8 kg m−2 h−1 under one-sun illumination—well above the classical thermal limit—while excluding 75% of the salt from 3.6 wt % brine and showing no surface crystallization. Its rapid hydration (swelling ratio of 4.22 in 30 s) ensures fast start-up, and its constituent polymers and agricultural by-products keep the raw materials cost below US$15 m^{-2}.

Zeolite A proved to be an excellent pollutant removal agent, eliminating 90% of contaminants in under 30 minutes at minimal dosage. This performance represents a

significant improvement over natural zeolites and, thanks to the simplicity of the synthesis materials, offers a rapid and cost-effective solution for water purification.

Titanium dioxide (TiO2) was evaluated for its photocatalytic capabilities and, when coupled with graphitic carbon nitride (g-C3N4), substantially enhances sunlight-driven degradation of organic pollutants. This TiO2/g-C3N4 composite can be applied across diverse wastewater streams while maintaining low production costs and exhibiting self-regeneration via photolytic breakdown of adsorbed species.

These findings support the viability of combining hydrogel- based desalination, zeolite adsorption, and photocatalysis into a fully solar-powered purification system suited for off-grid and low-resource settings. Future work will focus on optimizing the synthesis process, maximizing long-term performance under variable pollutant loads, and exploring alternative biodegradable polymers (e.g., chitosan derived from shrimp shells) to further advance sustainability in rural water treatment applications.

Together, these attributes position the PSA/PONI/Loofah hydrogel as a practical, stand-alone desalination medium for off-grid desert-edge and coastal settlements where reverse-osmosis infrastructure is unattainable

Acknowledgments

We are truly grateful to the strong support and mentorship provided by the teachers at our school. Dr. Shimaa Sobhy and Dr. Yousef Nagah. We extend special thanks to Dr. Khaled Abu-Zeid and the entire Water Projects team at CEDARE for their aid during the competition phase of the competition. We thank the doctors and researchers at the National Research Center, where we conducted our analysis. We are likewise indebted to the Stockholm International Water Institute (SIWI) for supervising the global SJWP program and for creating an opportunity for young water researchers.

References

Arun, J., Nachiappan, S., Rangarajan, G., Alagappan, R. P., Gopinath, K. P., & Lichtfouse, E. (2023). Synthesis and application of titanium dioxide photocatalysis for energy, decontamination and viral disinfection: A review. *Environmental Chemistry Letters, 21*, 339–362. https://doi.org/10.1007/s10311-022-01503-z

Atab, M. S., Smallbone, A., & Roskilly, A. P. (2016). An operational and economic study of a reverse osmosis desalination system for potable water and land irrigation. *Desalination, 397*, 174–184. https://doi.org/10.1016/j.desal.2016.06.020

Budiarso, I. J., Dabur, V. A., Rachmantyo, R., Judawisastra, H., Hu, C., & Wibowo, A. (2024). Carbon nitride- and graphene-based materials for the photocatalytic degradation of emerging water pollutants. *Materials Advances, 5*(8), 2668–2688. https://doi.org/10.1039/D3MA01078C

Chen, X., Liu, S., Yang, N., Yu, R., & Wang, D. (2023). Hierarchical structure regulation for sequential steps in solar vapor generation. *EcoMat, 5*(7), Article e12348. https://doi.org/10.1002/eom2.12348

Dehmani, Y., Mohammed, B. B., Oukhrib, R., Dehbi, A., Lamhasni, T., Brahmi, Y., *et al.* (2024). Adsorption of various inorganic and organic pollutants by natural and synthetic zeolites: A critical review. *Arabian Journal of Chemistry, 17*(1), Article 105474. https://doi.org/10.1016/j.arabjc.2023.105474

Gao, X., Sun, L., Hao, P., Zhang, S., Shen, Y., Hou, J., *et al.* (2024). Construction of black g-C_3N_4/loofah/chitosan hydrogel as an efficient solar evaporator for desalination coupled with antibiotic degradation. *Separation and Purification Technology, 355*, 129615. https://doi.org/10.1016/j.seppur.2024.129615

Hu, X., Yang, J., Tu, Y., Su, Z., Guan, Q., & Ma, Z. (2024). Hydrogel-based interfacial solar-driven evaporation: Essentials and trails. *Gels, 10*(6), 371. https://doi.org/10.3390/gels10060371

Kumari, S., Chowdhry, J., Kumar, M., & Garg, M. C. (2024). Zeolites in wastewater treatment: A comprehensive review on scientometric analysis, adsorption mechanisms, and

future prospects. *Environmental Research, 260*, 119782. https://doi.org/10.1016/j.envres.2024.119782

Puri, N., & Gupta, A. (2023). Water remediation using titanium and zinc oxide nanomaterials through disinfection and photocatalysis process: A review. *Environmental Research, 227*, 115786. https://doi.org/10.1016/j.envres.2023.115786

Vatansever, K. (2024, August 21). Covering the Sahara Desert with solar energy: A solution for net zero? *Carbon Gate*. https://www.carbongate.io/en/blog/sahra-colu-nu-gunes-enerjisiyle-kaplamak-net-zero-icin-cozum-mu

Wang, X., Zhang, L., Zheng, D., Xu, X., Bai, B., & Du, M. (2023). A polyelectrolyte hydrogel-coated loofah sponge evaporator based on Donnan effect for highly efficient solar-driven desalination. *Chemical Engineering Journal, 462*, 142265. https://doi.org/10.1016/j.cej.2023.142265

Yue, Y., Wang, Y., Bai, Y., Han, J., Cheng, W., Han, G., *et al.* (2023). A loofah-based all-day-round solar evaporator with phenolic lignin as the light-absorbing material for highly efficient photothermal conversion. *Chemical Engineering Journal, 477*, 147298. https://doi.org/10.1016/j.cej.2023.147298

Zeng, J., Wang, Q., Shi, Y., Liu, P., & Chen, R. (2019). Osmotic pumping and salt rejection by polyelectrolyte hydrogel for continuous solar desalination. *Advanced Energy Materials, 9*(38), Article 1900552. https://doi.org/10.1002/aenm.201900552

Zhang, C., Liang, H.-Q., Xu, Z.-K., & Wang, Z. (2019). Harnessing solar-driven photothermal effect toward the water–energy nexus. *Advanced Science, 6*(18), Article 1900883. https://doi.org/10.1002/advs.201900883

Zhou, X., Guo, Y., Zhao, F., Shi, W., & Yu, G. (2020). Topology-controlled hydration of polymer network in hydrogels for solar-driven wastewater treatment. *Advanced Materials, 32*(52), Article 2007012. https://doi.org/10.1002/adma.202007012